RSC Advances

This is an *Accepted Manuscript*, which has been through the Royal Society of Chemistry peer review process and has been accepted for publication.

Accepted Manuscripts are published online shortly after acceptance, before technical editing, formatting and proof reading. Using this free service, authors can make their results available to the community, in citable form, before we publish the edited article. This *Accepted Manuscript* will be replaced by the edited, formatted and paginated article as soon as this is available.

You can find more information about *Accepted Manuscripts* in the Information for Authors.

Please note that technical editing may introduce minor changes to the text and/or graphics, which may alter content. The journal's standard Terms & Conditions and the Ethical guidelines still apply. In no event shall the Royal Society of Chemistry be held responsible for any errors or omissions in this *Accepted Manuscript* or any consequences arising from the use of any information it contains.

ROYAL SOCIETY OF CHEMISTRY

www.rsc.org/advances

Journal Name

RSCPublishing

COMMUNICATION

Vapour-based processing of hole-conductor-free $CH_3NH_3PbI_3$ perovskite/C_{60} fullerene planar solar cells

Cite this: DOI: 10.1039/xoxxoooooox

Hao Hu,[a,c] Dong Wang,[a,c] Yuanyuan Zhou,[b] Jiliang Zhang,[d] Siliu Lv,[a] Shuping Pang,[a,*] Xiao Chen,[a] Zhihong Liu,[a] Nitin P. Padture,[b] Guanglei Cui [a,*]

Received ooth January 2012,
Accepted ooth January 2012

DOI: 10.1039/xoxxoooooox

www.rsc.org/

A new sequential-vapour-deposition method is demonstrated for the growth of high-quality $CH_3NH_3PbI_3$ perovskite films. This has enabled the all-vapour, low-temperature fabrication of hole-conductor free planar perovskite solar cells consisting of only a $CH_3NH_3PbI_3/C_{60}$ bi-layer sandwiched between two electrical contacts, with a power conversion efficiency of 5.4%.

Organometallic trihalide perovskites with the general formula $(RNH_3)MeX_3$ (where R is an organic group, Me is Pb or Sn, and X is a halogen I, Br, or Cl) have recently emerged as new generation light harvesting materials in excitonic solar cells.[1-3] In particular, methylammonium (*MA*) lead triiodide ($CH_3NH_3PbI_3$ or *MA*PbI_3) has attracted great deal of attention since it was first applied as the light absorber in mesoscopic solar cells.[4-6] Within a short period of time the power conversion efficiency (PCE) of *MA*PbI_3-based solar cells has shot up dramatically to 16.2%.[4,6,7] This rapid rise in the performance is the result of the innate desirable properties of *MA*PbI_3, including favourable direct band gap, large adsorption coefficient, high carrier mobilities and long carrier (balanced) diffusion lengths.[1,5,6,8] With regards to the latter, Xing *et al*.[8] showed that the carrier diffusion length in solution-processed *MA*PbI_3 thin films is at least 100 nm, despite the non-ideal nature of the solution-spun *MA*PbI_3 films. Higher PCEs of ~12% were obtained by Malinkiewicz *et al*.[9] and Chen *et al*.[10] in planar (non-mesoscopic) solar cells based on better quality *MA*PbI_3 films of ~300 nm thickness. This suggests that maximizing the quality (coverage, crystallinity, texture) of *MA*PbI_3 films can lead to carriers diffusion lengths >300 nm, which is the key to realizing planar perovskite-based solar cells with high efficiencies.[8, 9]

However, reliable deposition of high-quality films of phase-pure *MA*PbI_3 perovskites with full coverage and high crystallinity still remains a challenge.[5,6] One-step solution-spun *MA*PbI_3 generally results in films with pinholes due to high reaction rate between *MA*I and PbI_2.[4,10] To address this issue Burschka, *et al*.[4] developed a two-step method, where mesoporous TiO_2 is first infiltrated by solution-processed PbI_2, followed by dipping it in a *MA*I solution for the *in situ* formation of *MA*PbI_3. However, in the case of planar solar cells, where a mesoporous TiO_2 scaffold is not used, several hours are needed for the complete conversion of *MA*PbI_3, which can result in the peeling of the films.[4] In another study involving planar solar cells, the dipping process was replaced by extended annealing of the solution-processed PbI_2 film in a *MA*I-vapour-rich N_2 atmosphere at 150 °C [10]. However, this process may be not amenable to producing uniform *MA*PbI_3 films on organic substrates.[10] Meanwhile, Liu *et al*.[11] and Malinkiewicz *et al*.[9] used dual-source co-evaporation deposition to prepare uniform, pinhole-free films of *MA*PbI_3 or chorine-doped *MA*PbI_3, where the resulting planar solar cells delivered one of the highest PCEs. However, careful control of evaporation rates of the organic and the inorganic precursors is needed to achieve proper stoichiometry in the deposited films.

To that end, we demonstrate here a facile sequential-vapour-deposition (SVD) approach for the growth of high-quality *MA*PbI_3 films, which has enabled the fabrication of simple perovskite-based planar solar cells consisting of a *MA*PbI_3 perovskite/C_{60} fullerene bi-layer sandwiched between two electrical contacts (indium tin oxide (ITO) coated glass and thermally-evaporated Ag). A maximum PCE of 5.4 % is achieved in these solar cells. To our knowledge, this type of bi-layer architecture, which is devoid of any additional blocking layer, any mesoporous scaffold (*e.g.* TiO_2, ZnO, or Al_2O_3), and any additional conducting organic layers, constitutes the simplest perovskite-based working solar cell reported thus far. Especially, while several groups have hole-conductor-free mesoscopic perovskite solar cells, this is the first report of planar perovskite solar cells without use of hole conductors.

Figure 1 is a schematic diagram of the SVD method for the growth of *MA*PbI_3 films. A nanostructured porous PbI_2 film is first

[a] Qingdao Institute of Bioenergy and Bioprocess Technology, Chinese Academy of Sciences, Qingdao 266101, P.R. China
E-mail: pangsp@qibebt.ac.cn; cuigl@qibebt.ac.cn
[b] School of Engineering, Brown University, Providence, RI 02912, USA
[c] University of Chinese Academy of Sciences, Beijing 100049, P. R. China
[d] Department of Physics and Materials Science, City University of Hong Kong, Hong Kong SAR
Electronic Supplementary Information (ESI) available. See DOI: 10.1039/c000000x/

RSC Advances Accepted Manuscript

vapour-deposited (Fig. 1A), followed by the vapour-deposition of *MA*I (Fig. 1B), which reacts *in situ* with the PbI_2 film (Fig. 1C). The freshly prepared *MA*PbI_3 film is further annealed at 100 °C for 30 min to produce a textured film (Fig. 1D). Note that strong texture in perovskite films have been suggested to be beneficial, most likely due to their improved carriers-transport properties.[12,13]

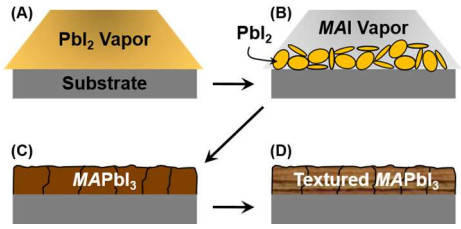

Figure 1. Schematic representation of the sequential-vapour deposition (SVD) process for the growth of *MA*PbI_3 perovskite films.

Detailed experimental procedures, including SVD growth of the films and solar cells fabrication, are presented in the accompanying Electronic Supplementary Information (ESI). Also presented in ESI are characterization procedures, including X-ray diffractometry (XRD), scanning electron microscopy (SEM), optical microscopy and ultraviolet-visible (UV-*vis*) optical spectroscopy, and procedures for solar cells testing.

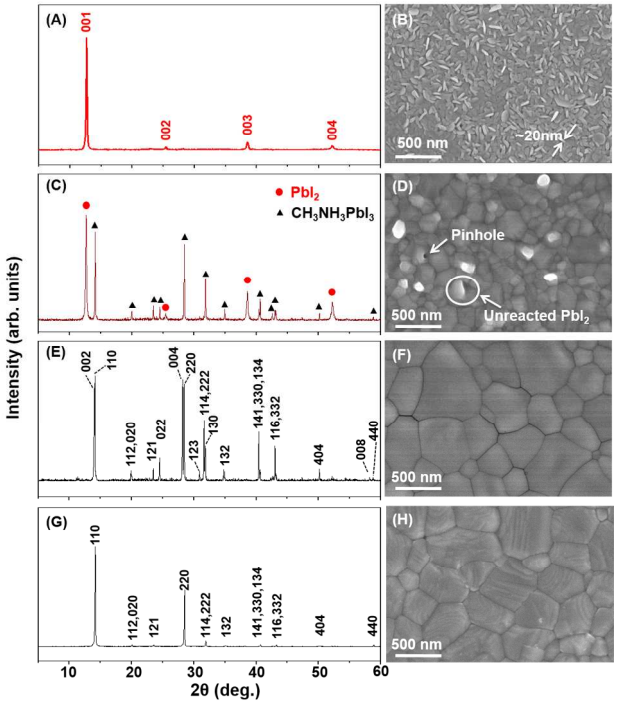

Figure 2. Indexed XRD patterns and corresponding SEM images (top surface) of films at the different stages during SVD growth: (A, B) after PbI_2 vapour deposition; (C, D) partially reacted with *MA*I vapour (5 min); (E, F) fully reacted with *MA*I vapour (15 min); (G, H) after annealing at 100 °C for 30 min.

Figure 2 shows XRD patterns from the films at different stages of the SVD growth, and the evolution of the surface morphology of the thin films. The XRD pattern in Fig. 2A confirms the presence of orthorhombic PbI_2 (space group *P3m1*; a=4.600(2) Å, b=4.600(2) Å, c=6.9926(9) Å) in the film after the first step, and shows a strong 001 texture. The corresponding SEM image in Fig. 2B shows full-coverage, smooth film consisting of randomly-oriented packing of plate-like PbI_2. There is significant amount of porosity between the adjacent PbI_2 plates in the film. The thickness of the PbI_2 plate-like structures is estimated at ~20-30 nm (see Fig. S1 in ESI), which is responsible for the broadening of the XRD peaks in Fig. 2A. In contrast, solution-processed PbI_2 films prepared by spin-coating are relatively rough, with equiaxed grains of PbI_2 of few hundred nanometers size.[4] Figure 2C is XRD pattern of PbI_2 film exposed to *MA*I vapour for 5 min, showing the presence of both PbI_2 and *MA*PbI_3. The corresponding SEM image in Fig. 2D shows features such as unreacted PbI_2 and pinholes. Visually, the side exposed to *MA*I vapour appears black (*MA*PbI_3), while the back side appears yellow (PbI_2) through the glass. This indicates that the PbI_2+*MA*I → *MA*PbI_3 reaction is diffusion limited. After additional 10 min of *MA*I vapour exposure the reaction is complete, as confirmed by XRD (Fig. 2E); the XRD pattern shows phase-pure tetragonal *MA*PbI_3 (space group *I4/mcm*; a=b=8.8745(7) Å, c=12.665(2) Å) and the absence of PbI_2. The corresponding SEM image (Fig. 2F) shows a uniform, smooth film of polycrystalline *MA*PbI_3 with a grain size of ~500 nm. The entire thickness (~350 nm) of the *MA*PbI_3 film appears black visually. Heat-treatment (100 °C, 30 min.) of the *MA*PbI_3 perovskite film results in the development of strong 110 texture (Fig. 2G), and a slightly distorted structure (a=8.876(5), b=8356(2) Å, c=12.530(6) Å). SEM image in Fig. 2H shows no grain coarsening as a result of the heat-treatment, but shows faceting of the individual grains. How this texture develops during this modest heat-treatment is not know at this time.

It appears that the nanoporous nature of the vapour-deposited PbI_2 film (Fig. 2B), with its large specific surface area, allows easy ingress and contact with *MA*I vapour, promoting rapid and more uniform reaction between PbI_2 and *MA*I. This results in phase-pure *MA*PbI_3 films that are pinhole-free, uniform, and smooth (Fig 2F). Since the film thickness is ~350 nm, and the size of the *MA*PbI_3 grains is ~500 nm, most of the *MA*PbI_3 grains span the entire thickness of the film. In other words, majority of the grain boundaries in the SVD-processed *MA*PbI_3 films are expected to run vertically between the substrate and the film surface, and that the horizontal grain boundaries across the path of carriers transport are likely to be in the minority.

Figure 3A shows the UV-*vis* absorbance spectrum of the *MA*PbI_3 perovskite film (on ITO) prepared by the SVD method and the corresponding differential transmission ($\Delta T/T$) spectrum (inset is an optical photograph showing black film). The $CH_3NH_3PbI_3$ perovskite film exhibits strong adsorption of UV-*vis* light up to ~790 nm wavelength, which is consistent with what is reported in the literature.[8,14,15] However, from the differential transmission spectrum, the SVD-processed $CH_3NH_3PbI_3$ perovskite film shows only one intense photobleaching peak at ~760 nm which is assigned to the direct band gap transition. The broad absorption peak at ~480 nm, which is typically observed in *MA*PbI_3 perovskite films, is virtually absent in the $\Delta T/T$ spectrum in Fig. 3A. This is probably related to different band structure in the SVD-processed *MA*PbI_3 perovskite films that exhibits unique crystal morphology. These distinct UV-*vis* absorption characteristics of the SVD-processed *MA*PbI_3 perovskite films also indicate the likelihood of an efficient photo-induced charge transfer during the solar cell operation.[16]

Figure 3B is a color-enhanced cross-sectional SEM image of a typical *MA*PbI_3/C_{60} bilayer solar cell fabricated in this study, illustrating the simple cell architecture. All three layers — *MA*PbI_3, C_{60}, Ag — are vapour deposited (see ESI). The energy-levels diagram of this simple cell architecture is shown in the Fig. 3C inset. Here the *MA*PbI_3 film serves as absorber, electron-donor, hole-conductor, and electron-blocking layer. Whereas the C_{60} layer serves as electron-acceptor, electron-conductor, and hole-blocking layer.

RSC Advances Accepted Manuscript

This journal is © The Royal Society of Chemistry 2012

Since MAPbI$_3$ is a good hole-conductor, additional hole-conducting layers typically used in perovskite-based solar cells can be eliminated while retaining high PCEs.[17-19] Furthermore, the widely used mesoporous TiO_2 electron-acceptor/-conductor scaffold and/or dense TiO_2 hole-blocking layer, which require high-temperature processing, have been eliminated in these solar cells.[17-19] Efficient electron-hole dissociation occurs at the MAPbI$_3$/C$_{60}$ interface, making C$_{60}$ a promising candidate as a non-oxide electron-acceptor/-conductor and hole-blocking layer in perovskite-based solar cells.[14,15]

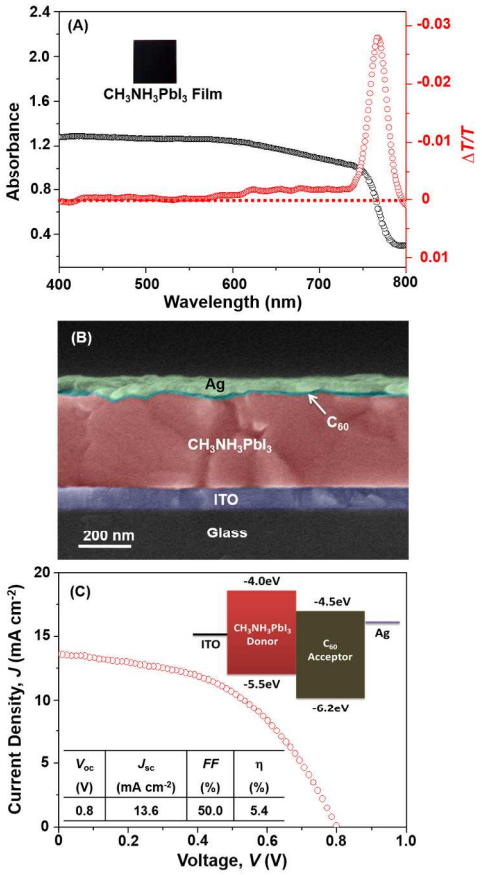

Figure 3. (A) UV-*vis* absorption spectrum and transformed differential transmission spectrum of MAPbI$_3$ perovskite film (inset: optical photograph). (B) Cross-sectional SEM image of a MAPbI$_3$/C$_{60}$ solar cell (false color). (C) Current density (J) – voltage (V) response of a MAPbI$_3$/C$_{60}$ solar cell under AM1.5G one sun illumination (top inset: energy-levels diagram; bottom inset: extracted solar cell performance parameters).

Figure 3C shows a typical current density (J) - voltage (V) response of the MAPbI$_3$/C$_{60}$ bilayer solar cell under AM1.5G simulated one sun illumination, and the solar-cell performance parameters are reported in the inset. Ten solar cells were tested, and their performance data are summarized in Table S1 (see ESI), with the PCE ranging from 4.1% to 5.4%. Considering the simplicity of these solar cells, a maximum PCE of 5.4%, an open-circuit voltage (V_{OC}) of 0.8 V, and a short circuit current density (J_{SC}) of 13.6 mA.cm^{-2}, are promising, and they can be attributed to the high quality of the SVD-processed MAPbI$_3$ films. The estimate of the maximum V_{OC} is given by [14]:

$$Voc \approx \left(\left|E_{\text{Donor}}^{\text{HOMO}}\right| - \left|E_{\text{Acceptor}}^{\text{LUMO}}\right|\right)/e \qquad (1)$$

Substituing the values from the energy-levels diagram in Fig. 3C (inset) in Eqn. 1, the maximum V_{OC} is estimated at 1.0 V for the MAPbI$_3$/C$_{60}$ heterojunction, representing a 20% loss in the measured V_{OC} (0.8 V) in the MAPbI$_3$/C$_{60}$ bi-layer solar cell (Fig 3C).

Jeng *et al.* [14] and Chiang *et al.* [20] report PCEs of 1.6% and 3.62%, respectively, for solution-processed MAPbI$_3$/C$_{60}$ solar cells, but their solar cells also contain additional layers of poly(3,4-ehylenedioxythiophene) poly(styrene-sulfonated) (PEDOT:PSS) and bathocuproine (BCP). The PEDOT:PSS layer is the hole transporter and it is necessary for solution processing of MAPbI$_3$[18], and the BCP layer is used as a hole-blocker. The voltage loss in MAPbI$_3$/C$_{60}$ solar cells by Jeng *et al.* [17] is 45%, whereas cells by Chiang *et al.* [10] show a lower loss of 16%. The use of a layer of a C$_{60}$ derivate — (6,6)-phenyl-C$_{61}$-butyric acid methyl ester (PC$_{61}$BM) — instead of the C$_{60}$ layer, in solution-processed MAPbI$_3$/PC$_{61}$BM solar cells results in higher PCE (7.4%) [18], however, those cells also use the additional layer of PEDOT:PSS. The maximum estimated V_{OC} for these MAPbI$_3$/PC$_{61}$BM is 1.23 V, and the measured V_{OC} in those cells is 0.91 V [18] or a 26% loss. Thus, the voltage loss in the simple MAPbI$_3$/C$_{60}$ bi-layer solar reported here is one of the lowest for solar cells based on MAPbI$_3$/fullerene heterojunctions, which is attributed to the improved coverage of perovskite film by SVD method.

With regard to J_{SC}, the measured value of 13.6 mA.cm^{-2} reported here is the highest among all the MAPbI$_3$/fullerene heterojunction solar cells reported so far [14,15,20]. This is attributed to the relatively thicker and denser SVD-processed MAPbI$_3$ films used here that are able to absorb light more efficiently. The fill factor (FF) of 50% is relatively low in these MAPbI$_3$/C$_{60}$ solar cells, which could be due to various factors, including non-ideal electrical contacts. Thus, there is a plenty of room for improvement in this regard through further optimization of the ITO surface and the C$_{60}$/Ag interface.

Conclusions

An SVD method is demonstrated for the growth of high-quality MAPbI$_3$ films, and the possible growth mechanisms are elucidated. This constitutes a new contribution to the menu of processing methods available for the growth of MAPbI$_3$ pervoskite films. The resulting MAPbI$_3$ films are pinhole-free, uniform and smooth, and most of the textured MAPbI$_3$ grains within the films span the entire thickness of the film. The high quality of the MAPbI$_3$ films allowed us to fabricate hole-conductor-free planar MAPbI$_3$ perovskite solar cells at low temperature (100 ˚C maximum) that deliver a promising PCE of 5.4%, V_{OC} of 0.8 V, and J_{SC} of 13.6 mA.cm^{-2}, but a relatively low FF of 50%. While the simple bi-layer cell architecture is used here to demonstrate the efficacy of the SVD process, high-quality MAPbI$_3$ films grown by the SVD process can be used in more complex solar cell architectures for much higher performance, and also in other future optoelectronic devices.

Acknowledgements

This research was funded by the Chinese National Natural Science Foundation (grant no. 51202266), Natural Science Foundation of Shandong Province (ZR2013FZ001), the Research Program of Qingdao (13-1-4-228-jch, 12-1-4-9-(4)-jch, 12-4-1-24-gx) and the U.S. National Science Foundation (grant no. DMR-1305913).

Notes and references

1 G. Hodes, *Science*, 2013, **342**, 317-318.
2 B. V. Lotsch, *Angew. Chem. Int. Ed.*, 2014, **53**, 635-637.

RSC Advances Accepted Manuscript

3 S. Kazim, M. K. Nazeeruddin, M. Grätzel and S. Ahmad, *Angew. Chem. Int. Ed.*, 2014, **53**, 2812-2824.
4 J. Burschka, N. Pellet, S. J. Moon, R. Humphry-Baker, P. Gao, M. K. Nazeeruddin and M. Gratzel, *Nature*, 2013, **499**, 316-319.
5 N. G. Park, *J. Phys. Chem. Lett.*, 2013, **4**, 2423-2429.
6 H. S. Kim, S. H. Im and N. G. Park, *J. Phys. Chem. C*, 2014, **118**, 5615-5625.
7 A. Kojima, K. Teshima, Y. Shirai and T. Miyasaka, *J. Am. Chem. Soc.*, 2009, **131**, 6050-6051.
8 G. C. Xing, N. Mathews, S. Y. Sun, S. S. Lim, Y. M. Lam, M. Grätzel, S. Mhaisalkar and T. C. Sum, *Science*, 2013, **342**, 344-347.
9 O. Malinkiewicz, A. Yella, Y. H. Lee, G. M. Espallargas, M. Grätzel, M. K. Nazeeruddin and H. J. Bolink, *Nature Photon.*, 2014, **8**, 128-132.
10 Q. Chen, H. Zhou, Z. Hong, S. Luo, H. S. Duan, H. H. Wang, Y. Liu, G. Li and Y. Yang, *J. Am. Chem. Soc.*, 2014, **136**, 622-625.
11 M. Liu, M. B. Johnston and H. J. Snaith, *Nature*, 2013, **501**, 395-398
12 J. M. Ball, M. M. Lee, A. Hey and H. J. Snaith, *Energy Environ. Sci.*, 2013, **6**, 1739-1743
13 E. Edri, S. Kirmayer, A. Henning, S. Mukhopadhyay, K. Gartsman, Y. Rosenwaks, G. Hodes and D. Cahen, *Nano Lett.*, 2014, **14**, 1000-1004.
14 S. Y. Sun, T. Salim, N. Mathews, M. Duchamp, C. Boothroyd, G. C. Xing, T. C. Sum and Y. M. Lam, *Energy Environ. Sci.*, 2014, **7**, 399-407.
15 J. Y. Jeng, Y. F. Chiang, M. H. Lee, S. R. Peng, T. F. Guo, P. Chen and T. C. Wen, *Adv. Mater.*, 2013, **25**, 3727-3732.
16 A. Marchioro, J. Teuscher, D. Friedrich, M. Kunst , R. Krol, T. Moehl, M. Grätzel and J. E. Moser, *Nature Photon.*, 2014, **8**, 250-255.
17 L. Etgar, P. Gao, Z. S. Xue, Q. Peng, A. K. Chandiran, B. Liu, M. K. Nazeeruddin and M. Grätzel, *J. Am. Chem. Soc.*, 2012, **134**, 17396-17399.
18 W. Abu Laban and L. Etgar, *Energy Environ. Sci.*, 2013, **6**, 3249-3253.
19 J. Shi, J. Dong, S. Lv, Y. Xu, L. Zhu, J. Xiao, X. Xu, H. Wu, D. Li, Y. Luo and Q. Meng, *Appl. Phys. Lett.*, 2014, **104**, 063901.
20 Y. F. Chiang, J. Y. Jeng, M. H. Lee, S. R. Peng, P. Chen, T. F. Guo, T. C. Wen, Y. J. Hsu and C. M. Hsu, *Phys. Chem. Chem. Phys.*, 2014, **16**, 6033-6040.

RSC Advances Accepted Manuscript

 This journal is © The Royal Society of Chemistry 2012